Received February 24, 2019, accepted May 6, 2019, date of publication May 15, 2019, date of current version May 24, 2019.

Digital Object Identifier 10.1109/ACCESS.2019.2916888

Surface FGM Insulator Based on $BaTiO_3$ Magnetron Sputtering for Electric Field Grading of AC Gas Insulated Power Apparatus

BOXUE DU, (Senior Member, IEEE), ZEHUA WANG, JIN LI, (Member, IEEE), MI XIAO, AND HUCHENG LIANG

Key Laboratory of Smart Grid of Education Ministry, School of Electrical and Information Engineering, Tianjin University, Tianjin 300072, China

Corresponding authors: Jin Li (lijin@tju.edu.cn) and Hucheng Liang (hcliang@tju.edu.cn)

This work was supported in part by the National Natural Science Foundation of China under Grant 51807136 and Grant 51537008, in part by the Natural Science Foundation of Tianjin City under Grant 18JCQNJC07300 and Grant 18JCYBJC21700, in part by the National Postdoctoral Program for Innovative Talents under Grant BX201700168, and in part by the China Postdoctoral Science Foundation under Grant 2017M621070.

ABSTRACT Electric field optimization is a critical technique to ensure the compact structure and reliable operation for AC gas insulated power apparatus. To obtain a more uniform electric field distribution, this paper proposes the concept of the d-SFGM insulator, i.e., applying the surface functionally graded material (SFGM) with a designed thickness (d) distribution of high permittivity along the insulator surface. The magnetron sputtering technique was used to fabricate the d-uniform insulator and the d-SFGM insulator by depositing $BaTiO_3$ layers. The theoretical analysis indicates that the electric field distribution is optimized using the d-SFGM insulator, followed by the d-uniform insulator. The finite element simulations were employed to investigate the electric field distributions and dielectric losses of different insulators. The results show that for the case of the d-uniform insulator, a higher permittivity or larger thickness of the sputtering layer results in a more uniform electric field distribution. With the application of the d-SFGM insulator, the maximum electric field strength and dielectric loss are both significantly reduced compared to the d-uniform insulator. Finally, experimental tests were conducted to further verify the feasibility of SFGM. The AC flashover voltage of the d-SFGM insulator is much higher than those of the conventional insulator and the d-uniform insulators. Therefore, the d-SFGM insulator has great potential for improving the reliability of the AC gas insulated power apparatus.

INDEX TERMS Gas insulated power apparatus, insulator, surface functionally graded material, flashover, permittivity, magnetron sputtering.

I. INTRODUCTION

The gas insulated power apparatus plays an important role in the generation, transmission and distribution of the power energy, combining reliability with low losses, low electromagnetic interference, high transmission capacity and safety [1], [2]. Solid insulators made of epoxy/Al_2O_3 composites provide mechanical support and electrical insulation for AC gas insulated power apparatus [3]. However, flashover along the insulator surface can easily occur, thereby limiting the operating voltage level and threatening the security of the power system [4].

The associate editor coordinating the review of this manuscript and approving it for publication was Bora Onat.

Generally, the highly non-uniform electric field distribution along the insulator surface is considered an important cause of flashover [5]. Because of the higher relative permittivity of the solid insulator compared to the surrounding gas, the electric field is intensified along the gas-solid interface, especially at the triple junction [6]. Structural optimization of the solid insulator, including additional electrodes and complicated insulator shapes, has been applied to improve the distribution of electric field [7]. Nevertheless, these conventional techniques complicate the equipment structure and increase the manufacturing costs [8], [9]. Therefore, novel methods for grading the electric field and increasing the flashover voltage of insulators have recently been proposed.

The concept of functionally graded material (FGM) with a spatially inhomogeneous permittivity distribution was originally applied to insulator [10]. The laminating method was used to prepare the graded post-type insulator, whose flashover voltage under lightning impulse voltage was increased by 10-25% compared to that of the conventional insulator [11]. The centrifugation technique was then developed to fabricate permittivity (ε)-FGM conical insulators with a continuous permittivity distribution [12]–[15]. The results showed that the application of ε-FGM insulators can reduce the maximum electric field near the triple junction and increase the flashover voltage compared to ε-uniform insulators under lightning impulse voltage. Recently, 3D printing technology was used to fabricate FGM insulators; however, more research and development are required for industrial applications of such FGM epoxy insulators [16]–[18]. Existing fabrication processes such as lamination, centrifugation, and 3D printing show some limitations. First, the control range of permittivity for FGM insulator by bulk doping is small (4-80), which limits the effect of electric field regulation. Second, these methods not only degrade mechanical performances of insulators but also are complex, which makes the FGM insulators hard to be brought into the practical application.

To break the above limitations, the concept of d-SFGM, i.e., applying FGM to the insulator surface, was proposed to form thickness (d) gradient surface layers of ultrahigh permittivity. The radio-frequency (RF) magnetron sputtering technique was used to deposit $BaTiO_3$ layers on cone-type insulators to obtain the d-uniform and d-SFGM insulators. Subsequently, the fracture section was observed using a scanning electron microscope (SEM) to investigate the influence of sputtering time on the layer thickness. Then the dielectric parameters of sputtering layer were calculated from the capacitance and resistance measurements. Next, the effects of layer permittivity and thickness on electric field distribution and the dielectric loss of insulator were investigated via finite element simulations. Finally, the flashover voltages of the conventional, d-uniform and d-SFGM insulators were measured to verify the feasibility of SFGM.

II. CONCEPT OF SFGM

Figure 1 shows equivalent-circuit models for the conventional insulator (Figure 1a), d-uniform insulator (Figure 1b) and d-SFGM insulator (Figure 1c). The conventional insulator consists of epoxy/Al_2O_3 composites, whose volume relative permittivity is about 6.8. The d-uniform insulator consists of two parts: the bulk consisting of epoxy/Al_2O_3 composite with a low relative permittivity and the surface layer of $BaTiO_3$ with an ultrahigh relative permittivity (over 1000). When the thickness of the surface layer is designed to be functionally graded along the insulator surface, a d-SFGM insulator can be obtained. To simplify the model for easy understanding, the stray capacitance of air is ignored because the permittivity of air is quite low compared with the insulator and the $BaTiO_3$ layer.

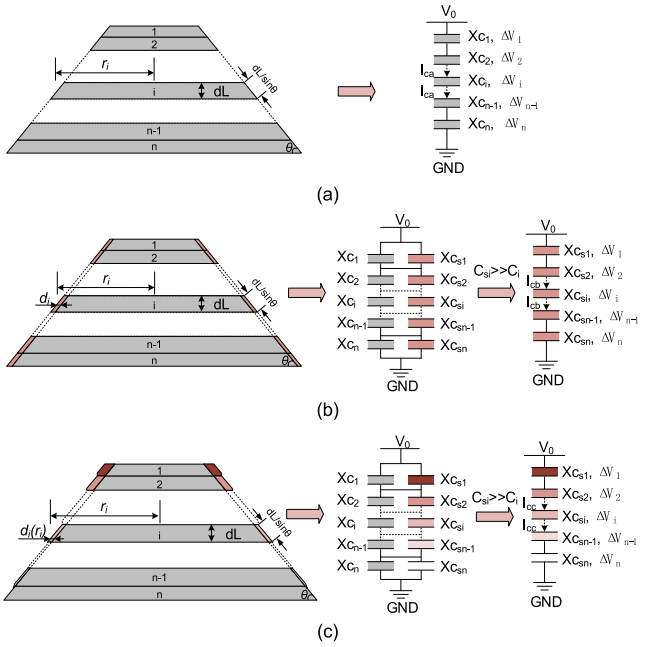

FIGURE 1. Equivalent-circuit models for cone-type insulators. (a) The conventional insulator, (b) the d-uniform insulator, and (c) the d-SFGM insulator.

As shown in Figure 1a, a cone-type insulator can be divided into n ($n \to \infty$) elements. Each element i can be regarded as a cylinder with a radius of r_i and a height of dL. Denoting the capacitance value of each element i as C_i, the conventional insulator can be approximately considered a capacitor series of C_i. According to the capacitance formula, the capacitance value of element i can be calculated as,

$$C_i = \frac{\varepsilon_0 \varepsilon_r \pi r_i^2}{dL} \tag{1}$$

where ε_0 and ε_r are the vacuum permittivity and the relative permittivity of the insulator, respectively. The capacitive reactance of element i can be calculated according to the following equation:

$$Xc_i = \frac{1}{2\pi f C_i} \tag{2}$$

where f is the power frequency, which is set to 50 Hz in this paper. Under AC voltage, the leakage current primarily consists of the capacitive current I_c. Without considering the conductive current, the electric potential drop dV_i across element i can be calculated as follows:

$$dV_i = I_c Xc_i \tag{3}$$

Based on the above analysis, the electric field strength E_i^a along element i surface of the conventional insulator can be described as,

$$E_i^a = \frac{dV_i}{dL/\sin\theta} = \frac{I_{ca}\sin\theta}{2\pi^2 f \varepsilon_0 \varepsilon_r} \cdot \frac{1}{r_i^2} \tag{4}$$

According to Equation (4), it can be inferred that the electric field distribution along the insulator surface is

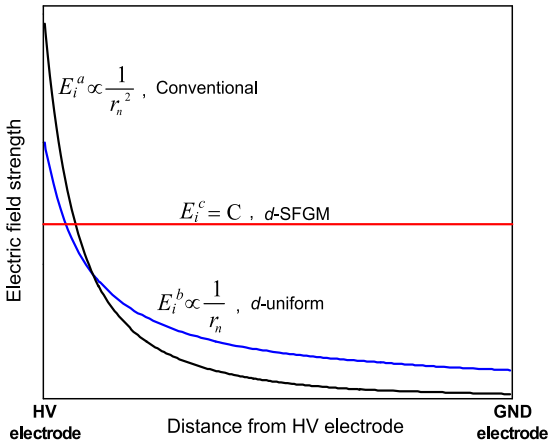

FIGURE 2. Ideal electric field distributions for cone-type insulators.

extremely uneven. The maximum electric field strength appears near the HV electrode and decreases from the HV electrode to the GND electrode.

For the d-uniform insulator as shown in Figure 1b, both the bulk and surface layer can be divided into n ($n \to \infty$) elements. Each element i of the surface layer can be regarded as a cylindrical ring with a radius of r_i, a thickness of d and a height of dL. According to the capacitance formula, the capacitance value of each surface layer element i can be approximately formulated as,

$$C_{si} = \frac{\varepsilon_0 \varepsilon_{rs} 2\pi r_i d}{dL} \tag{5}$$

where ε_{rs} is the relative permittivity of the surface layer. In the equivalent-circuit model for the d-uniform insulator, the bulk capacitor series and the surface layer capacitor series are connected in parallel. When $C_{si} \gg C_i$, the equivalent circuit can be simplified to only the surface layer capacitor series. The electric field strength E_i^b along element i surface of the d-uniform insulator can be expressed as,

$$E_i^b = \frac{dV_i}{dL/\sin\theta} = \frac{I_{cb}\sin\theta}{4\pi^2 f \varepsilon_0 \varepsilon_{rs} d} \cdot \frac{1}{r_i} \tag{6}$$

Compared with the conventional insulator, the electric field distribution along the d-uniform insulator is more uniform because the electric field strength is proportional to r^{-1} instead of r^{-2}, as shown by equations (6) and (4), respectively.

If the surface layer thickness is designed to be functionally graded along the insulator surface ($d(r_i) = \text{const}/r_i$), as shown in Figure 1c, then the electric field strength E_i^c along surface of element i of the d-SFGM insulator can be described as,

$$E_i^c = \frac{I_{cc}\sin\theta}{4\pi^2 f \varepsilon_0 \varepsilon_{rs} d\ (r_i)} \cdot \frac{1}{r_i} = \frac{const \cdot I_{cc}\sin\theta}{4\pi^2 f \varepsilon_0 \varepsilon_{rs}} \tag{7}$$

Equation (7) indicates that the electric field strength along the d-SFGM insulator is constant in the ideal case.

The ideal electric field distributions along the conventional insulator, d-uniform insulator and d-SFGM insulator are shown in Figure 2. Considering some idealized hypotheses have been made to simplify the model, the electric field distribution calculated by using the equivalent-circuit models have some deviations. Thus, the finite element simulation is necessary to obtain the accurate electric field distributions of insulators.

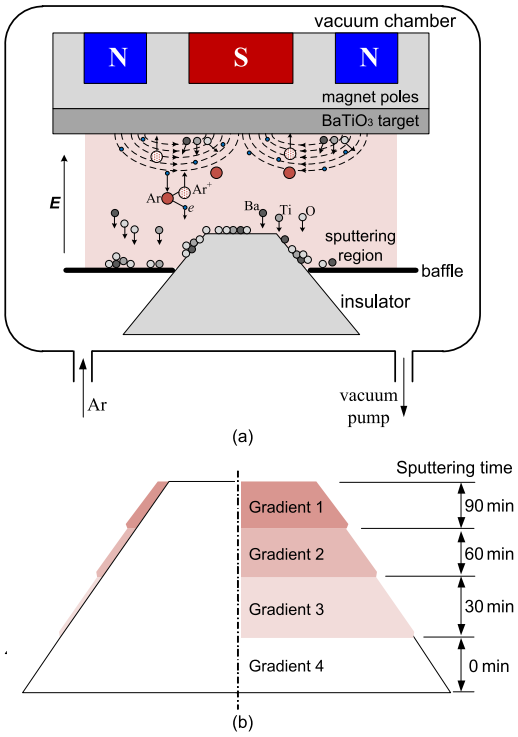

FIGURE 3. Preparation of sputtered insulators. (a) Experimental setup for $BaTiO_3$ magnetron sputtering of insulators. (b) Gradient arrangement along the insulator surface.

III. FABRICATION OF SFGM INSULATOR

A. MAGNETRON SPUTTERING

The cone-type insulators used in the experiments were comprised of epoxy/Al_2O_3 composites, produced following the industrial manufacturing process. In this paper, three d-uniform insulators and one d-SFGM insulator with $BaTiO_3$ as the deposition material were fabricated using an RF magnetron sputtering apparatus, including a JPGF-400 magnetron sputterer cooled with cold-water circulation, which has been widely used in the semiconductor processing field [19].

The experimental setup for magnetron sputtering of insulators is shown in Figure 3a. The $BaTiO_3$ target with the diameter of 60 mm and the thickness of 3 mm was provided by CHINO New Material Technology Co. Ltd. The cone-type insulator was placed below the $BaTiO_3$ target and remained intact during the sputtering process. By adjusting both the position and hole size of the baffle, the sputtering area of insulator can be controlled. Before sputtering, the chamber was evacuated to achieve the required pressure of less than 5×10^{-3} Pa. The input RF power was 90 W, and the gas flow rate of Ar:O_2 was set to 4:1 (SCCM). In the magnetron

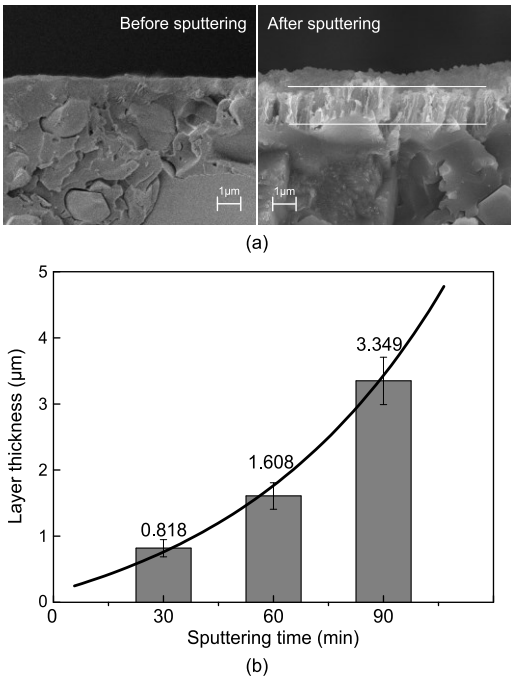

FIGURE 4. Effects of sputtering time on the sputtering layer thickness. (a) Cross-section SEM images of the insulators. (b) Relationship between the layer thickness and the sputtering time.

sputtering process, the target is bombarded by energetic gaseous ions generated by stable RF glow discharge plasma to cause the removal of target atoms, which then condense on insulators as a thin film [20]. Although secondary electrons move to the substrate, the magnetic field can restrict them to a nearby target, thus increasing the possibility of collision ionization of electrons and atoms. The increased ionization efficiency results in the increased ion bombardment on the target, giving higher sputtering rates and higher deposition rates on the substrate [20], i.e., the insulator.

For a constant sputtering power, the sputtering layer thickness is dependent on the sputtering time. To obtain d-uniform insulators with different layer thicknesses, the sputtering times of three d-uniform insulators were set to 30, 60 and 90 min. Figure 3b shows the surface gradient arrangement for the d-SFGM insulator. The cone-type insulator was divided into four gradients with equal height, and the sputtering times of each gradient were 90, 60, 30 and 0 min from top to bottom.

B. SURFACE MORPHOLOGY

Figure 4a shows the cross-sectional microstructure of cone-type insulators. For the untreated insulator, the Al_2O_3 filler was found to be in the form of a massive structure that was mixed in the epoxy. Compared with the conventional insulator, there is a distinct $BaTiO_3$ layer deposited on the sputtered insulator surface. Then the average layer thicknesses after 30, 60 and 90 min's sputtering process were measured. To further investigate the functional relationship between the sputtering layer thickness and the sputtering time, curve fitting was conducted, as shown in Figure 4b. With increasing sputtering

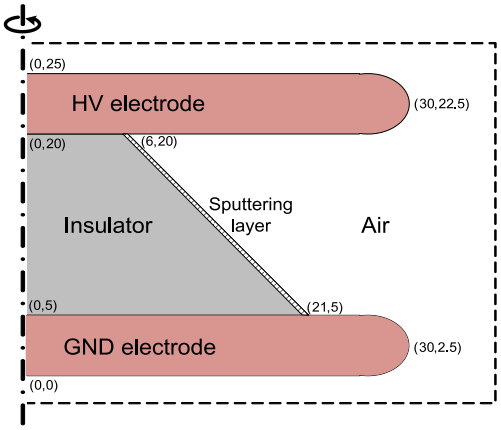

FIGURE 5. Simulation model for the cone-type insulator.

time, the sputtering layer thickness increases via the following exponential relationship [21]:

$$d = 1.046e^{\frac{t}{63.5}} - 0.9882 \tag{8}$$

where d is the thickness of the sputtering layer, μm, and t represents the sputtering time, min.

C. DIELECTRIC PARAMETERS MEASUREMENT

To obtain the permittivity and conductivity of the sputtering layer, the capacitance and resistance were measured using the (LCR) meter under 1 V AC voltage of 50 Hz. Under the same conditions as above, $BaTiO_3$ was deposited on a sheet copper to form an even layer for better accuracy of measurement results. Then another smaller electrode with diameter of 50 mm was pressed tightly on the sputtering layer. The $BaTiO_3$ permittivity value can be calculated according to the capacitance formula, which is about 1600 in this paper. Similarly, the volume conductivity of sputtering layer can be obtained from the measured resistance value, which is about 1×10^{-7} S/m.

IV. ELECTRIC FIELD SIMULATION

A. SIMULATION MODEL

Based on the Maxwell-Wagner theory, the finite element simulations were conducted to investigate the effects of the sputtering layer on electric field distribution of the solid insulator. Figure 5 shows the calculation model which is based on a rotationally symmetric system. In the figure, the physical dimensions of insulator and electrodes are presented in the form of coordinates in millimeters. An AC voltage of 15 kV was applied at the HV electrode. The governing equations for the electric calculation are as follows:

$$\nabla \cdot \boldsymbol{J} = 0 \tag{9}$$

$$\boldsymbol{J} = \sigma \boldsymbol{E} + j\omega \boldsymbol{D} \tag{10}$$

$$\boldsymbol{E} = -\nabla V \tag{11}$$

where $\boldsymbol{E}$ is the electric field strength, V/m; V is the electric potential, V; $\boldsymbol{J}$ is the current density, A/m^2; σ is the volume

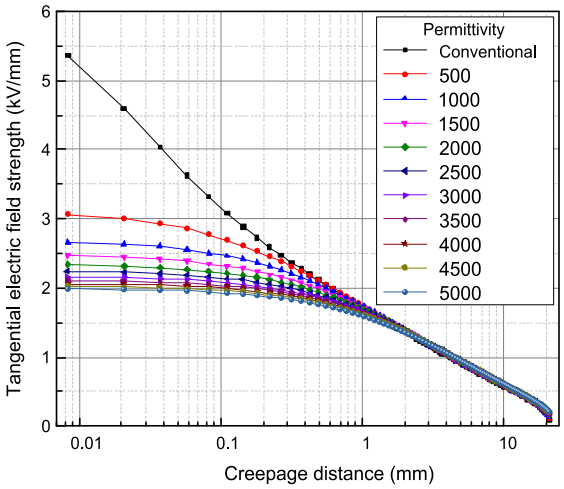

FIGURE 6. Electric field distributions along the conventional insulator and $BaTiO_3$-sputtered insulators with different layer permittivities.

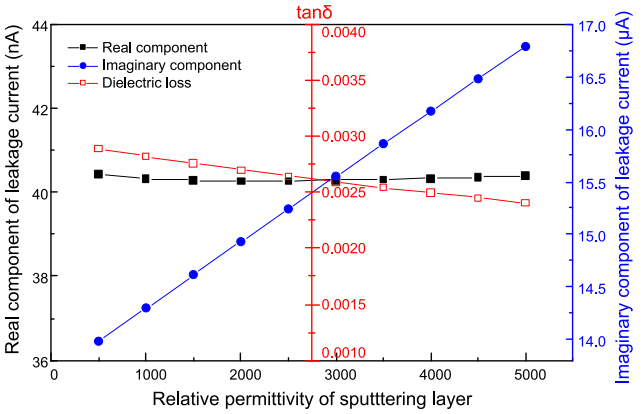

FIGURE 7. Leakage currents and dielectric losses of the $BaTiO_3$-sputtered insulator with different layer permittivities.

conductivity of the involved dielectrics, S/m; ω is the angular frequency of the power grid, rad/s; $\boldsymbol{D}$ is the electric flux density, C/m^2.

B. EFFECTS OF SPUTTERING LAYER PERMITTIVITY

Since the layer permittivity value can vary with preparation parameters such as sputtering gas, sputtering power and target purity, it is necessary to explore the effects of the sputtering layer permittivity on electric field distribution along the insulator surface, as shown in Figure 6. In this simulation, the thickness of the sputtering layer on the insulator surface is uniform, with a value of 4 μm. The relative permittivity is set to 500-5000. The creepage distance $l = 0$ mm is the location of the HV electrode, and the creepage distance $l = 21$ mm is the location of the GND electrode. The electric field strength declines from the HV triple junction to the GND triple junction. Therefore, the flashover is primarily triggered by the region surrounding the HV triple junction. To illustrate the electric field distribution near the HV triple junction, the logarithm of the creepage distance is presented. The maximum electric field strength at the triple junction clearly decreases with increasing permittivity of the sputtering layer. However, when the permittivity reaches a value of 3500, the electric field distribution is only slightly affected by the permittivity of the sputtering layer. The ''saturation effect'' of the relaxation function on electric field of the sputtering layer with high permittivity can be explained as follows. According to the equivalent-circuit model shown in Figure 1b, the capacitance value C_{si} of each surface layer element i increases with increasing permittivity of the sputtering layer. For a higher permittivity of the layer, the assumption of $C_{si} \gg C_i$ is more realistic, and the electric field distribution is more consistent with equation (6). When the permittivity reaches a certain value, the assumption of $C_{si} \gg C_i$ becomes true. Therefore, the continued growth of the layer permittivity has only a slight influence on the electric field distribution along the surface of the $BaTiO_3$-sputtered insulator.

Because the permittivity and conductivity of sputtering layer are both higher than those of epoxy/Al_2O_3 composites, it is meaningful to analyze the leakage current and dielectric loss of insulator. By integrating the current density on the HV or GND electrode, the leakage current of the insulator can be obtained. Figure 7 shows the real component (I_R) and imaginary component (I_C) of leakage currents as well as dielectric losses (tanδ) of the $BaTiO_3$-sputtered insulators with different levels of layer permittivity. As the relative permittivity of the sputtering layer varies from 500 to 5000, the imaginary component of insulator leakage current continues to increase from 14.0 to 16.9 μA, because of the increasingly lower capacitive reactance of sputtering layer; but the real component of leakage current almost keeps constant. As for the dielectric loss, the ration of I_R to I_C, has inevitable decline trend.

C. EFFECTS OF SPUTTERING LAYER THICKNESS

Figure 8 shows the electric field distributions along the conventional insulator and $BaTiO_3$-sputtered insulators with different sputtering layer thicknesses. The permittivity value of sputtering layer is set to 1600 in this section, and layer thickness ranges from 1 to 10 μm. By introducing the $BaTiO_3$ layer, the electric field strength is significantly reduced at the triple junction. With increasing layer thickness, the effect of the electric field relaxation function grows substantially. And when the layer thickness reaches 8 μm, the electric field distribution becomes stable. Similarly, the capacitance value C_{si} of element i increases with increasing thickness of the sputtering layer. For a thicker layer, the assumption of $C_{si} \gg C_i$ is more realistic, and the electric field distribution is more likely to obey equation (6). It is clear that when the layer thickness reaches a certain value, the assumption of $C_{si} \gg C_i$ will hold true. The electric field changes slightly with the layer thickness, and the ''saturation effect'' of the electric field relaxation function appears again. As shown in Figure 9, the maximum electric field strength declines

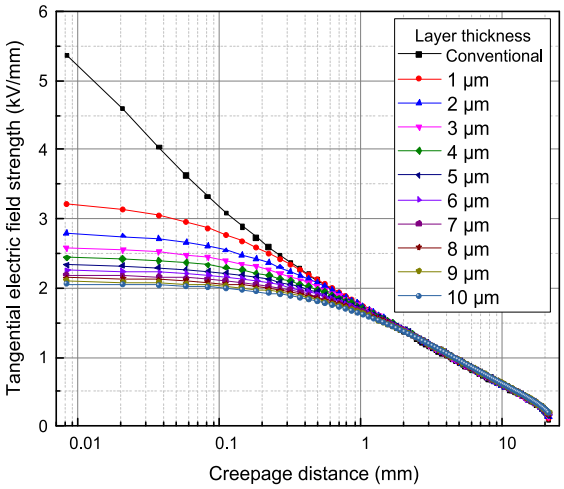

FIGURE 8. Electric field distributions along the conventional insulator and $BaTiO_3$-sputtered insulators with different layer thicknesses.

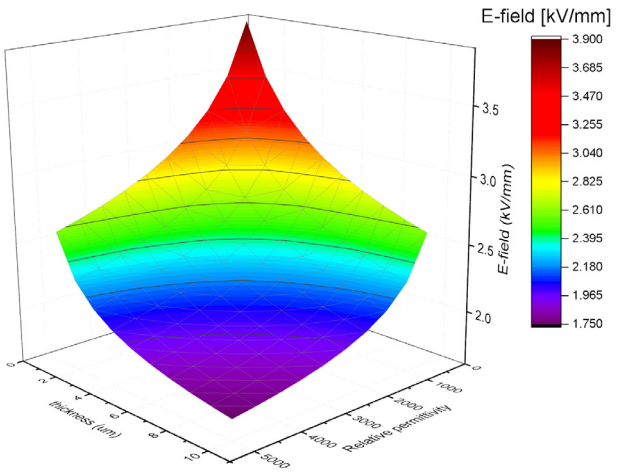

FIGURE 9. Combined effects of sputtering layer permittivity and thickness on maximum electric field strength along insulator surface.

with increasing both the sputtering layer permittivity and thickness, and finally reaches a stable value when the product of sputtering layer permittivity and thickness is high enough.

Figure 10 shows the leakage currents and dielectric losses of the $BaTiO_3$-sputtered insulators with different layer thicknesses. The thicker sputtering layer, the increasingly reduced capacitive reactance and impedance of the sputtering layer causes the $BaTiO_3$-sputtered insulator to have a larger I_C and I_R. Meanwhile, the rising rate of I_R is higher than that of I_C, which causes increased loss of insulator. In practical applications, an optimal sputtering layer thickness should be chosen by considering both the electric field distribution and the dielectric loss.

D. APPLICATION OF PREPARED INSULATORS

As described, the "saturation effect" of the electric field relaxation function exists in the d-uniform insulator with increasing permittivity and/or thickness of the sputtering layer. For superior electric field distribution, the

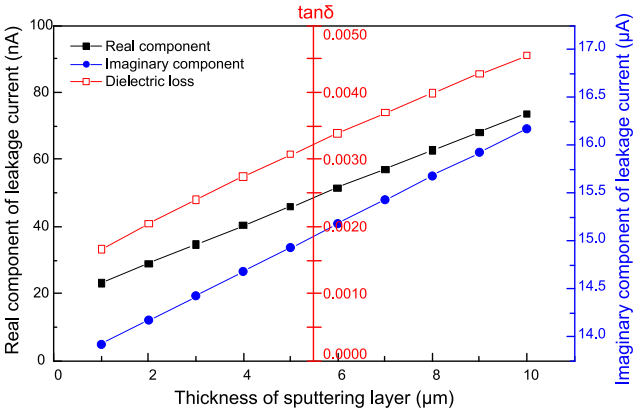

FIGURE 10. Leakage currents and dielectric losses of the $BaTiO_3$-sputtered insulators with different layer thicknesses.

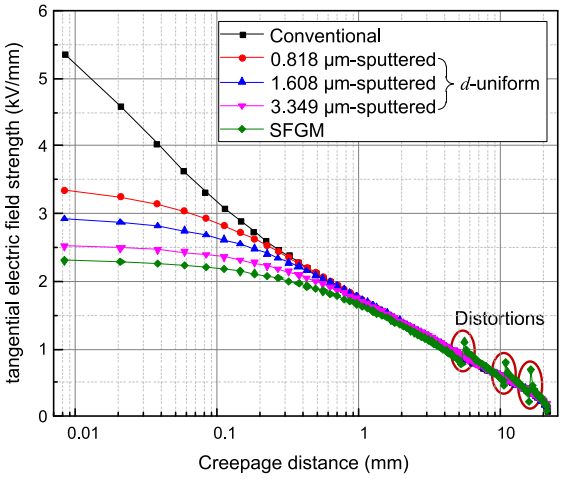

FIGURE 11. Electric field distributions along the conventional, d-uniform and d-SFGM insulators.

d-SFGM insulator is necessary to be presented. The prepared insulators, three d-uniform insulators and a d-SFGM insulator, were applied to compare the electric field relaxation function and dielectric losses of insulators. Figure 11 shows the electric field distributions along the conventional insulator, d-uniform insulators and d-SFGM insulator. The permittivity of sputtering layer is 1600, which has been measured in front section. According to the theoretical analysis, to further improve the electric field distribution compared to the d-uniform insulator, the d-SFGM insulator was fabricated by grading the thickness of sputtering layer, as shown in Figure 3b. It is obvious that the maximum electric field strength at the HV triple junction is further reduced by the application of d-SFGM insulator compared with d-uniform insulators. Because of the thickness variations of the different gradients of sputtering layers, three electric field distortions can be observed. The electric field distortions can be suppressed by increasing the division of the gradient. Especially, the continuously graded distribution of sputtering layers could completely eliminate these distortions, because there is no mutation in thickness.

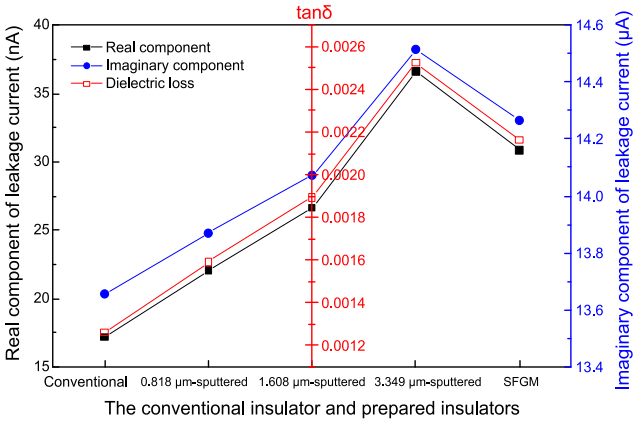

FIGURE 12. Leakage currents and dielectric losses of four kinds of prepared insulators.

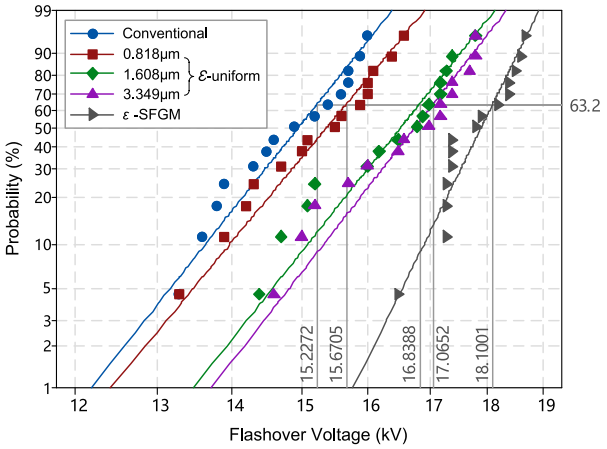

FIGURE 13. Weibull distributions of flashover voltages of the conventional insulator, ε-uniform insulators and ε-SFGM insulator.

In addition to the enhanced effect of relaxation on electric field strength, the d-SFGM insulator is also found to possess a lower leakage current and dielectric loss than the 3.349 μm-sputtered insulator, as shown in Figure 12. Therefore, the d-SFGM insulator has a greater potential for application in AC gas insulated power apparatus.

V. FLASHOVER TEST RESULTS

In the previous sections, the feasibility of the d-uniform insulator and the d-SFGM insulator with $BaTiO_3$-sputtered layers to achieve a uniform electric field distribution has been validated via theoretical analysis and electrical simulation. In this section, flashover tests were conducted to evaluate the insulation performance of insulators.

The test insulator was placed between parallel plane electrodes with a diameter of 60 mm. One of the electrodes was connected with a standard AC voltage through a limiting resistance, and the other with the ground. The AC flashover test was conducted in a chamber at the temperature of 20°C. At least fifteen flashover tests were performed for each kind of insulator. Then the Weibull plots were used to analyze the flashover voltages of the conventional insulator, d-uniform insulator and d-SFGM insulator.

Figure 13 shows the flashover voltages of the conventional insulator, d-uniform insulators (0.818-, 1.608-, and 3.349-μm-sputtered insulators) and the d-SFGM insulator. The observed phenomena are consistent with the electric field distribution. For the conventional insulator, the flashover voltage is ∼15.2 kV. The flashover voltage of the d-uniform insulator is higher than that of the conventional insulator and increases with increasing layer thickness. Among the d-uniform insulators, the 3.349 μm-sputtered insulator has the highest flashover voltage of ∼17.1 kV. By applying the d-SFGM insulator, the lower electric field strength near the HV triple junction causes the flashover voltage to reach as high as ∼18.1 kV. Such promotion of 20% on insulator flashover voltage is of great significance to prolong service life, save space and reduce GHG emission for AC gas insulated power apparatus. If the d-distribution is refined, according to equation (7), the flashover voltage of d-SFGM insulator can be significantly improved.

VI. CONCLUSIONS

The concept of SFGM was proposed and applied to cone-type insulators in this paper. The electric field distributions, leakage currents, dielectric losses and flashover voltages of the conventional insulator, d-uniform insulator and d-SFGM insulator were investigated. The main conclusions of this paper are as follows:

(1) The equivalent-circuit models indicate that the d-SFGM insulator has the most uniform electric field distribution, followed by the d-uniform insulator and the conventional insulator.

(2) For the d-uniform insulator, as the permittivity of the sputtering layer increases, the electric field distribution becomes increasingly uniform, and the dielectric loss of insulator decreases. As the sputtering layer thickness increases, the electric field distribution is increasingly improved. Considering the ''saturation effect'' of layer thickness on electric field relaxation, an optimal thickness should be designed to achieve the better electric field distribution and lower dielectric loss.

(3) Compared with the d-uniform insulators, by the introduction of the d-SFGM insulator, the maximum electric field strength at the HV triple junction is further reduced, with much lower dielectric loss.

(4) Flashover tests confirm that the d-SFGM insulator has the highest AC flashover voltage compared with the conventional insulator and the d-uniform insulator. Therefore, the d-SFGM insulator has great potential for practical application in AC gas insulated power apparatus.

REFERENCES

[1] H. Koch, F. Goll, T. Magier, and K. Juhre, ''Technical aspects of gas insulated transmission lines and application of new insulating gases,'' *IEEE Trans. Dielectr. Electr. Insul.*, vol. 25, no. 4, pp. 1448–1453, Aug. 2018.

[2] K. D. Srivastava and M. M. Morcos, "A review of some critical aspects of insulation design of GIS/GIL systems," in *Proc. IEEE/PES Transmiss. Distrib. Conf. Expo.*, Atlanta, GA, USA, Nov. 2001, pp. 787–792.
[3] B. X. Du *et al.*, "Temperature dependent surface potential decay and flashover characteristics of epoxy/SiC composites," *IEEE Trans. Dielectr. Electr. Insul.*, vol. 25, no. 2, pp. 631–638, May 2018.
[4] B. Du, Q. Du, J. Li, and H. Liang, "Carrier mobility and trap distribution dependent flashover characteristics of epoxy resin," *IET Gener., Transmiss. Distrib.*, vol. 12, no. 2, pp. 466–471, Jan. 2018.
[5] B. X. Du, H. C. Liang, J. Li, and Z. Y. Ran, "Electrical field distribution along SG_6/N_2 filled DC-GIS/GIL epoxy spacer," *IEEE Trans. Dielectr. Electr. Insul.*, vol. 25, no. 4, pp. 1202–1210, Aug. 2018.
[6] M. Talaat, A. El-Zein, and M. Amin, "Electric field simulation for uniform and FGM cone type spacer with adhering spherical conducting particle in GIS," *IEEE Trans. Dielectr. Electr. Insul.*, vol. 25, no. 1, pp. 339–351, Feb. 2018.
[7] W. A. Stygar *et al.*, "Improved design of a high-voltage vacuum-insulator interface," *Phys. Rev. Accel. Beams*, vol. 8, no. 5, May 2005, Art. no. 050401.
[8] K. Kato, M. Kurimoto, H. Shumiya, H. Adachi, S. Sakuma, and H. Okubo, "Application of functionally graded material for solid insulator in gaseous insulation system," *IEEE Trans. Dielectr. Electr. Insul.*, vol. 13, no. 2, pp. 362–372, Apr. 2006.
[9] M. Kurimoto, K. Kato, M. Hanai, Y. Hoshina, M. Takei, and H. Okubo, "Application of functionally graded material for reducing electric field on electrode and spacer interface," *IEEE Trans. Dielectr. Electr. Insul.*, vol. 17, no. 1, pp. 256–263, Feb. 2010.
[10] S. Watanabe *et al.*, "Electrical applications of titanium-based FGMs manufactured by progressive lamination," in *Proc. IEEE 6th Int. Conf. Conduction Breakdown Solid Dielectr. (ICCBSD)*, Vasteras, Sweden, Jun. 1998, pp. 539–542.
[11] N. Hayashi, K. Kawahara, M. Sumikura, M. Hara, and F. Endo, "Electric field control by permittivity functionally graded materials and their lightning impulse withstand voltages for surface breakdown," in *Proc. IEEE Int. Symp. Elect. Insul. (ISEI)*, Boston, MA, USA, Apr. 2002, pp. 260–263.
[12] N. Hayakawa, J. Shimomura, T. Nakano, M. Hanai, K. Kato, and H. Okubo, "Fabrication technique of permittivity graded materials (FGM) for disk-type solid insulator," in *Proc. Annu. Rep. Conf. Elect. Insul. Dielectr. Phenomena (CEIDP)*, Montreal, QC, Canada, Oct. 2012, pp. 32–35.
[13] N. Hayakawa, Y. Miyaji, H. Kojima, and K. Kato, "Electric field reduction by functionally graded materials (FGM) with permittivity and conductivity distribution," in *Proc. IEEE Conf. Elect. Insul. Dielectr. Phenomena (CEIDP)*, Toronto, ON, Canada, Oct. 2016, pp. 627–630.
[14] J. Ishiguro, M. Kurimoto, H. Kojima, K. Kato, H. Okubo, and N. Hayakawa, "Electric field control in coaxial disk-type solid insulator by functionally graded materials (FGM)," in *Proc. IEEE Conf. Elect. Insul. Dielectr. Phenomena (CEIDP)*, Des Moines, IA, USA, Oct. 2014, pp. 663–666.
[15] N. Hayakawa, J. Ishiguro, H. Kojima, K. Kato, and H. Okubo, "Fabrication and simulation of permittivity graded materials for electric field grading of gas insulated power apparatus," *IEEE Trans. Dielectr. Electr. Insul.*, vol. 23, no. 1, pp. 547–554, Feb. 2016.
[16] Z. Liu *et al.*, "Topology optimization and 3D-printing fabrication feasibility of high voltage FGM insulator," in *Proc. IEEE Int. Conf. High Voltage Eng. Appl. (ICHVE)*, Chengdu, China, Sep. 2016, pp. 1–4.
[17] Z. Liu, W.-D. Li, L.-Y. Zhang, X.-R. Li, J.-B. Deng, and G.-J. Zhang, "Simulation design and 3D-printing fabrication of conductivity graded insulator," in *Proc. IEEE 1st Int. Conf. Elect. Mater. Power Equip. (ICEMPE)*, Xi'an, China, May 2017, pp. 171–174.
[18] M. Kurimoto, H. Ozaki, Y. Yamashita, T. Funabashi, T. Kato, and Y. Suzuoki, "Dielectric properties and 3D printing of UV-cured acrylic composite with alumina microfiller," *IEEE Trans. Dielectr. Electr. Insul.*, vol. 23, no. 5, pp. 2985–2992, Oct. 2016.
[19] Y. Imanishi, M. Taguchi, and K.-I. Onisawa, "Effect of sublayer surface treatments on ZnO transparent conductive oxides using dc magnetron sputtering," *Thin Solid Films*, vol. 518, no. 11, pp. 2945–2948, Mar. 2010.
[20] P. J. Kelly and R. D. Arnell, "Magnetron sputtering: A review of recent developments and applications," *Vacuum*, vol. 56, no. 3, pp. 159–172, 2000.
[21] F. Gao and J. An, "BST thin films deposited by RF-magnetron sputtering and dielectric property research," in *Proc. IEEE Adv. Inf. Manage., Commun., Electron. Automat. Control Conf. (IMCEC)*, Xi'an, China, Oct. 2016, pp. 1808–1811.

BOXUE DU (SM'04) is currently a Professor and the Director–Founder of the School of Electrical and Information Engineering, Institute of High Voltage, Tianjin University, China. His research interests include dielectric failure mechanisms of polymer insulating materials, electrical insulation technology, and application of polymer dielectrics under various extreme environments, such as cryogenic, high temperature, high altitude, gamma-ray irradiation, and high-intensity magnetic field. He has published three books and eight book chapters in Polymer Dielectrics, and authored about 450 papers and more than 130 of them published in the IEEE Transactions. He has also served industry and start-ups as a consultant. He is an Editorial Boards Member of *IET High Voltage*, *Chinese Journal of High Voltage Engineering*, the *Journal of Modern Power Systems and Clear Energy*, the *Journal of Electrical Engineering*, and the *Journal of Insulating Materials*. He is a Fellow of IET, and a member at several WG in CIGRE. He is an Associate Editor of the IEEE TRANSACTIONS ON DIELECTRICS AND ELECTRICAL INSULATION, the IEEE ACCESS, and *IET Nanodielectrics*.

ZEHUA WANG was born in Taiyuan, China, in 1995. She received the B.S. degree from the Taiyuan University of Technology, China, in 2017. She is currently pursuing the master's degree with the School of Electrical Engineering and Automation, Tianjin University. Her current research interests include the fabrication and evaluation of FGM insulator in HVAC GIS/GIL.

JIN LI (M'17) was born in Tangshan, China, in 1988. He received the B.S. and Ph.D. degrees in electrical engineering from Tianjin University, China, in 2012 and 2017, respectively, where he is currently an Associate Professor with the School of Electrical and Information Engineering. His research interests include the designing and improvement of solid dielectrics for HVDC power cable, and gas-insulated transmission line.

MI XIAO was born in Baoding, China. He received the Ph.D. degree in electronic & information engineering from Tianjin University, China, in 1999, where he is currently an Associate Professor with the Department of Electrical Engineering, School of Electrical and Information Engineering. His research interest includes synthesis and the application of electronic functional ceramic materials.

HUCHENG LIANG was born in Nanyang, China, in 1992. He received the B.S. degree in electrical engineering from Tianjin University, China, in 2015, where he is currently pursuing the Ph.D. degree with the School of Electrical Engineering and Automation. His current research interests include the insulation and mechanical failures of GIS/GIL.